Directed Growth of Electroactive Metal-Organic Framework Thin Films Using Electrophoretic Deposition

Idan Hod, Wojciech Bury, David M. Karlin, Pravas Deria, Chung-Wei Kung, Michael J. Katz, Monica So, Benjamin Klahr, Danni Jin, Yip-Wah Chung, Teri W. Odom, Omar K. Farha, and Joseph T. Hupp**

Electrophoretic deposition (EPD) is used for the patterned growth of metal-organic framework (MOF) thin films on conductive surfaces. We find that deposition of pre-synthesized particles (microcrystallites) of the representative MOF materials,HKUST-1, Al-MIL-53, UiO-66 and NU-1000, from toluene suspensions and onto conductive glass can be readily accomplished without altering particle composition or degrading particle integrity. For NU-1000, which contains a redox-active linker, we find that with proper attention to film density all linkers within a film can be electrochemically addressed. These findings, especially if extended to other MOFs or to modified versions of the current MOFs, suggest that electrophoretic deposition will prove broadly useful for imparting to MOFs electrocatalytic and/or photoelectrochemical activity.

Metal organic frameworks (MOF) have engendered enormous scientific interest due to their routinely high porosities and surface areas, and due to their extraordinarily broad chemical and structural diversity.[1–3] Indeed, one of the most compelling features of MOFs as materials class is that their structures and compositions, and hence chemical properties,canbe broadly engineered via careful selection of: a)synthesis conditions/methodology, and b) molecular and ionic building blocks.[4] These features have motivated investigations of MOFs, typically in microcrystalline powder form,for a wide variety of applications, including gas storage,[5–8] chemical separations,[9] and chemical catalysis.[10,11] For other applications—for example, electrocatalysis,[12] chemical sensing,[13] batteries,[14] supercapacitors[15] and electrochromic devices—a more desirable form may be thin films.[16–18] Several approaches to MOF thin-film formation have now been explored, at least in preliminary fashion. The approaches include:surface-initiated solvothermal growth,[19–21] layer-by-layer assembly (also termed liquid-phase epitaxy),[22–24] substrate corrosion and/or reactive electrodeposition,[25–28] microwave-induced thermal deposition[29] and dip coating from colloidal solutions.[30] While each has its virtues, none has yet proven universally applicable or nearly so. Thus, there is a need for additional deposition methods—especially ones that are simple and broadly applicable, or at least applicable to MOFs that appear poorly suited to the methods noted above.

Electrophoretic deposition (EPD) is a well-established technique for fabricating thin films, especially from nanoparticulate building blocks. The application of a DC electric field to a suspension of charged particles in a nonpolar solvent can result in particle transport and deposition onto a conductive substrate. EPD has previously been employed to deposit semiconducting,[31–35] metallic[36–38] and insulating[39,40] nanoparticles on conductive platforms.

Here we report the electrophoresis-driven formation and growth of MOF thin films. The potential generality of the EPD method was demonstrated by the successful deposition of four representative MOFs: the Zr-based materials, NU-1000[41] and UiO-66[42] (see **Figure 1**a and b); the iconic Cu-based MOF, HKUST-1;[43] and the aluminum-based form of MIL-53[44] (see Figures S1 and S2). Notably, the deposited materials are characterized by distinctly different topologies, porosities, morphologies, sizes of crystallites, and degrees of chemical stability. During the material synthesis, all 4 types of MOFs present some surface defects (possibly due to missing linkers or missing metal nodes) that will give rise to some partial charges on the surface of the MOFs. During EPD process, those partial charges drive the particles toward the oppositely charged electrode. In practice, all of the examined MOFs display net negative charges and were deposited on the positively charged electrode. When the polarity of the electrodes was switched, as expected, the MOF particles were deposited on the opposite electrode, supporting the fact that the charged surfaces of the MOF materials drive their deposition. Finally, to further test the usefulness of EPD,we examined the feasibility of: a) depositing micropatterned films, and b) depositing two types of MOFs on a single conductive support.

Figure 1c illustrates a typical EPD procedure. First, two identical fluorine-doped tin oxide (FTO) transparent conductive electrodes are immersed in a colloidal MOF deposition suspension

Dr. I. Hod, Dr. W. Bury, Dr. D. M. Karlin, Dr. P. Deria, C. W. Kung, Dr. M. J. Katz, M. So, Dr. B. Klahr, Prof. T. W. Odom, Prof. O. K. Farha, Prof. J. T. Hupp
Northwestern University
Chemistry Department
60208, USA
E-mail: j-hupp@northwestern.edu
Dr. W. Bury
Department of Chemistry
Warsaw University of Technology
Noakowskiego 3 00-664, Warsaw, Poland
Dr. D. Jin, Prof. Y.-W. Chung
Northwestern University
Department of Materials Science and Engineering
60208, USA
Prof. O. K. Farha
Department of Chemistry
Faculty of Science, King Abdulaziz University
Jeddah, Saudi Arabia
E-mail: o-farha@northwestern.edu

DOI: 10.1002/adma.201401940

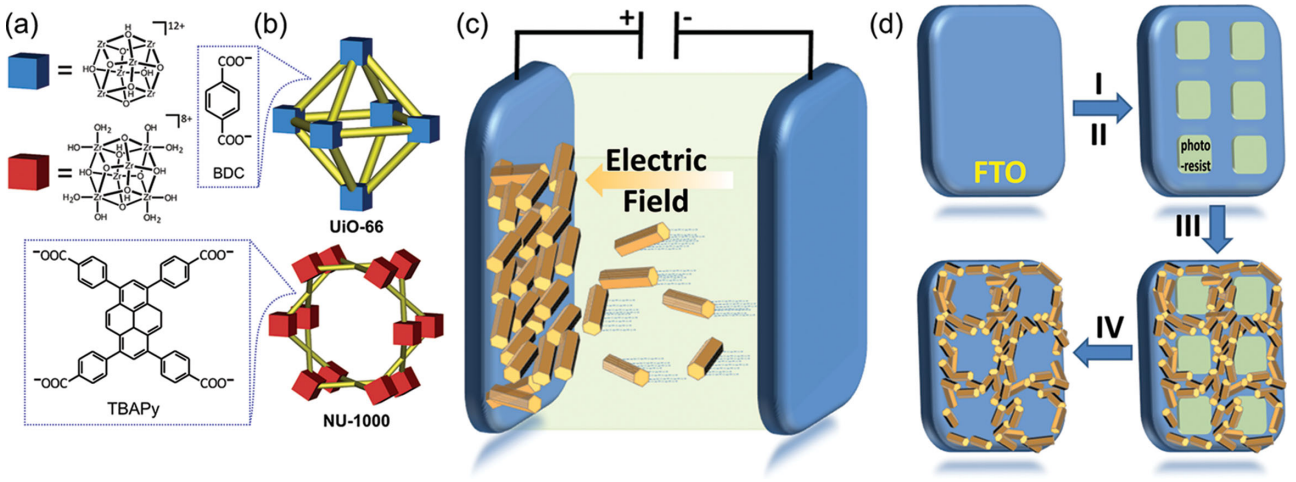

Figure 1. a) Components of UiO-66 and NU-1000: Zr-containing nodes (blue for UiO-66 and red for NU-1000) and organic linkers, b) illustration of the crystal structures of UiO-66 and NU-1000 MOFs c) a scheme illustrating the principal of MOFs EPD film growth, showing the attraction of charged MOF particles toward an oppositely charged electrode using an applied electric field d) illustration of the patterning of MOF EPD film procedure: I) spin coating a layer of photoresist on a bare FTO substrate, II) using photolithography to create patterned squares of photoresist, III) deposition of MOF particles on the conductive exposed FTO areas using EPD, and IV) removal of the remaining photoresist squares to obtain the desired pattern

approximately 1 cm apart from one another. Second, taking advantage of the fact that the suspended MOF particles possess a surface charge, a fixed voltage is applied between the two electrodes. In a low polarity, non ionizing solvent the applied voltage creates an electric field that drives the particles toward the oppositely charged electrode and ultimately deposits them.

As mentioned earlier, we have demonstrated the flexibility of the EPD technique by depositing four types of MOFs thin films, HKUST-1, Al-MIL-53, UiO-66 and NU-1000. For the remaining part of this work, we have concentrated our attention on the two Zr-based MOFs with different particle sizes to act as model systems since Zr-MOFs recently attracted a great deal of attention in several potential applications.[45–50] Moreover, we wanted to assess the suitability of EPD for depositing MOFs with particle sizes ranging from a few micrometers down to several hundreds of nanometers. To do so, we were able to fabricate thin films made of two kinds of Zr-based MOFs, micron sized crystals of $Zr_6(\mu_3\text{–}OH)_8(OH)_8(TBAPy)_2$(NU-1000)($H_4$TBAPy = 1,3,6,8-tetrakis(p-benzoic acid)pyrene) and nano sized crystalline particles of $Zr_6O_4(OH)_4(BDC)_2$UiO-66 (H_2BDC = 1,4-benzenedicarboxylic acid), as illustrated in Figure 1a and b. UiO-66 was synthesized solvothermally according to a previously published procedure while NU-1000 was synthesized using a slightly modified version of literature procedures, in which the $ZrOCl_2{\times}8H_2O$ was used as a Zr precursor instead of $ZrCl_4$ (see Supporting Information for experimental details).[41,42] For each MOF, thin film deposition suspensions were prepared by weighing 10 mg of the as-prepared MOF powder into a 20 ml toluene solution which was then sonicated for 30 s in order to form a homogenous colloidal dispersion of MOF particles. In **Figure 2**a, optical images of both UiO-66 and NU-1000 films deposited on FTO glass are presented (after 3 h of EPD), showing the characteristic yellow and white-colored films of NU-1000 and UiO-66 respectively. Upon UV excitation, we observe the emission from the fluorescent TBAPy pyrene-based ligand of NU-1000, while no emission is seen from the BDC ligand of the UiO-66 (Figure 2b). SEM images of both thin films were obtained displaying the rod-shaped hexagons and low aspect ratio crystal habits, which are characteristic for NU-1000 and UiO-66, respectively (Figure 2c and d include SEM images of the MOF thin films while Figure S3 includes SEM images of the bulk MOF crystals). Furthermore, in order to verify that the material deposited on the FTO electrodes retains its structural integrity, PXRD measurements of the films were collected. The deposited films retained the same crystal structure as the bulk NU-1000, UiO-66, Al-MIL-53, and HKUST-1 starting materials (Figure 2e, f, and S1).

To gain more insight into the effect of electrophoresis time on the characteristics of the deposited films, such as thickness and extent of surface coverage, we prepared a series of NU-1000 EPD films with different deposition times: a) 20 min b) 40 min c) 60 min d) 120 min and e) 180 min. Representative SEM images (top view) of the different films are presented in Figure S4 of the Supporting Information. It is clear that after 20 min of deposition, the surface coverage by the NU-1000 MOF crystals is low and a significant portion of the FTO is still exposed. As the deposition time increases, the fraction of FTO remaining exposed decreases, and after 180 min, the surface is essentially covered with MOF microcrystallites, as can be seen in **Figure 3**e. Additional data indicating that the deposition time determines the amount of material assembled on the surface was provided by measuring the PXRD patterns of films deposited at different times (Figure 3a). Qualitatively, we see that the relative diffraction peak intensities increase as a function of time, implying that more material had been deposited on the FTO substrate. Furthermore, cross sectional SEM image of the NU-1000 films grown for 3 h (Figure 3f) shows the random orientation of MOF particles on the electrode surface, with an approximate film thickness of 4–5 μm.The mechanical stability of the resulting NU-1000 EPD thin films was assessed using a scratching test utilizing a Micro Materials nanoscratch/nanoindentor. We have calculated the elastic modulus, as well

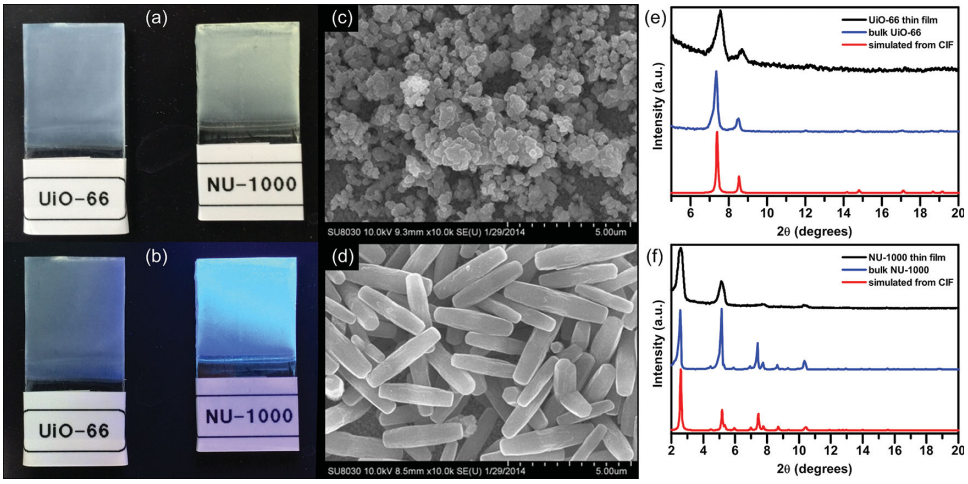

Figure 2. a) an optical micrograph of NU-1000 and UiO-66 films grown using EPD b) optical micrograph of NU-1000 and UiO-66 films under UV excitation, showing the emission of the pyrene based ligand of NU-1000 c-d) SEM images of UiO-66 and NU-1000 EPD films showing their typical crystal morphologies e-f) XRD patterns of UiO-66 and NU-1000 films, both matching the simulated and bulk crystal structures of each MOF.

as the maximum shear and tensile stresses at delamination of the film. The shear and tensile stresses are 1.4% and 0.6% of the elastic modulus respectively, suggesting that the EPD films have respectable adhesion on conducting glass substrates see Supporting Information for experimental details and results).

With an eye toward possible electrochemical applications,[51–53] we wanted to obtain insights regarding the conductivity and charge transfer properties of the prepared EPD films. Recently, we have shown that solvothermally grown NU-901 MOF films containing redox active pyrene moieties exhibit reversible electrochromism when the underlying FTO electrode is stepped to an electrochemical potential positive enough for the one electron oxidation of the pyrene linkers.[16] Taking into account that the building blocks for the synthesis of NU-1000 and NU-901 are identical (Zr node with the H_4TBAPy ligand), we wanted to explore the electroactivity of EPD films through the reversible redox reaction of the pyrene-based ligands. Cyclic voltammetry (CV) measurements of NU-1000 films, prepared over EPD times ranging from 20 min to 180 min, are shown on Figure 3b. The voltammograms were acquired using a standard three-electrode configuration featuring a Ag/AgCl reference electrode, a Pt-mesh counter electrode, and in a 0.1 M $TEAPF_6$ solution in CH_2Cl_2 as a supporting electrolyte. For all studied films, a chemically reversible redox reaction could be observed, with an anodic peak for the pyrene linker oxidation to a radical cation state at applied potentials of 1.2–1.4 V, followed by a reductive (cathodic) peak at potentials of 0.8–1.0 V that returns the pyrene to neutral form. Increases in current for both oxidation and reduction peaks were observed as the deposition time increased. For a given deposition time, the amount of linker displaying electroactivity was determined by integrating the oxidative voltammetry peak to obtain the charge passed and then

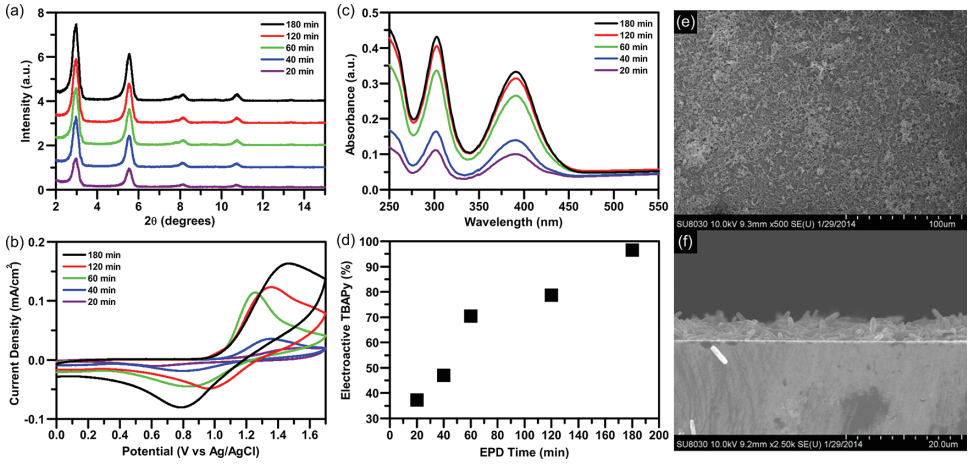

Figure 3. a) XRD plots for thin films of NU-1000 grown with different duration of EPD. b) CVs of NU-1000 film grown with different EPD duration, showing the reversible redox behaviour of the pyrene-containing linker. c) Absorption spectra of films of NU-1000, showing the increase in the total amount of surface-immobilized pyrene with deposition time.d) Plot of the precentage of electroactive pyrenes on the surface in relation to deposition duration, demonstrating the fact that upon reaching a complete surface coverage, practically all the pyrene could be electroactivated e) Top view SEM images of an NU-1000 film grown using 180 min of EPD. f) Cross sectional SEM image of an NU-1000 film obtained based on 180 min of EPD.

converting the charge to moles by assuming removal of one electron from each pyrene molecule displaying electroactivity. Total numbers of pyrene units present were determined by recording electronic absorption spectra of solutions of digested films in aq. 1 M NaOH, as shown in Figure 3c. The required molecular extinction coefficient of $TBAPy^{4-}$ in 1 M NaOH solution was determined from the slope of an absorption calibration curve (at 391 nm), as shown in Figure S5. For each of the MOF EPD films, the total amount of pyrene present and the amount exhibiting electroactivy were determined (Figure S6). The overall findings are summarized in Figure 3d which presents a plot of the percentage of material exhibiting electroactivity versus the deposition time, where time is proxy for the amount of MOF deposited. Strikingly, it can be seen that the percentage of electroactive pyrene increases with the deposition time, reaching a value of greater than 95% after 180 min. We interpret the findings to mean that not all deposited particles achieve good electrochemical contact with the conductive-glass electrode, but that particle-particle redox communication is effective. Thus, at loadings where most particles physically contact other particles, only a modest fraction needs to achieve direct electrochemical communication with the electrode itself in order for the overwhelming majority of particles to be effectively electrochemically addressable.

Desiring to challenge the EPD method and assess its ability for directing the deposition of MOF particles to predefined locations, we set out to construct patterned films. Fabrication of such patterned, surface-supported MOF structures could be useful for applications ranging from chemical sensing to electrical signaling. By combining photolithography with EPD, we were able to fabricate a micropatterned MOF thin film (see Figure 1d). Briefly, a layer of an insulating photoresist material was prepared on a bare FTO platform by spin coating (Figure 1d, process I). Photolithography was then used to create a patterned photoresist surface exhibiting a 25 μm diameter squares with 25 μm spacing (Figure 1D, process II). The next step involved EPD of MOF particles on the conductive exposed sections of FTO between the photoresist squares (Figure 1D, process III). Finally, removal of the remaining photoresist was done by immersing the film in acetone for 1 hour, leaving behind a patterned grid of MOF particles (Figure 1D, process **IV**). Representative SEM images of the resulting patterned MOF grid films are shown in **Figures 4**a and c and Figure S7 (Supporting Information). The images show the deposition of hexagonal NU-1000 MOF rods in grid-like fashion around square FTO areas. The features of the grid are in good size- and shape-agreement with the original pattern, i.e., lines approximately 25 μm wide, with ca. 25 μm spacing between them, with the pattern resolution limited by the MOF particle size. Upon irradiation with light from a 405 nm laser, strong pyrene luminescence from the patterned MOF material can be clearly observed as shown in the fluorescence microscopy image in Figure 4b. Additionally, the grids were observed to function as diffraction gratings for transmitted visible light (diffraction

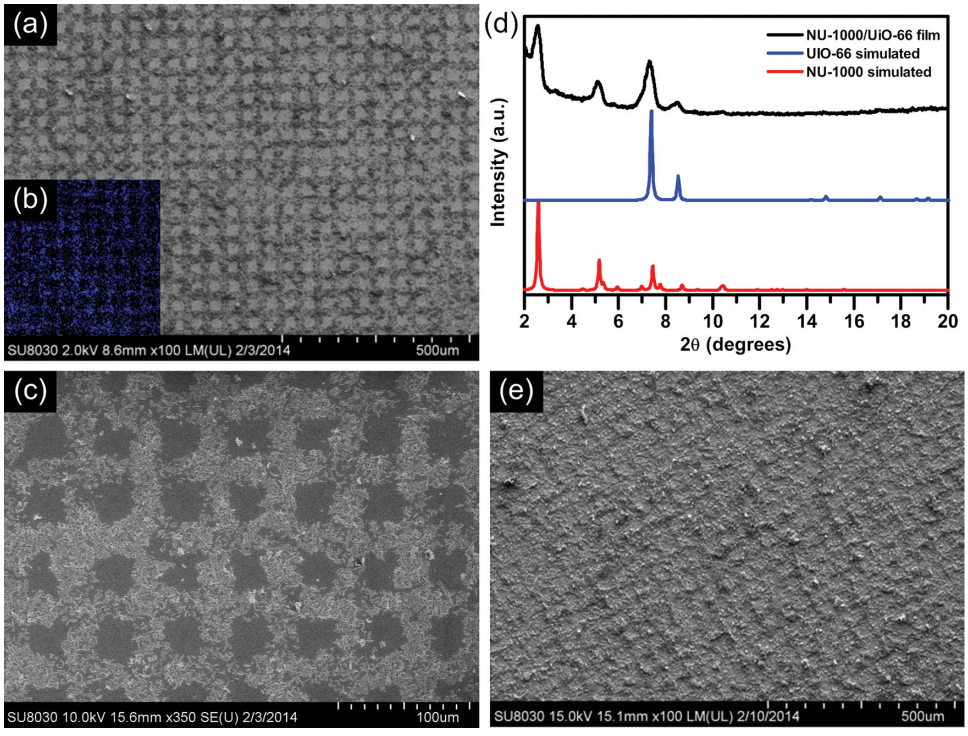

Figure 4. a) SEM image of a patterned MOF film showing grid lines of MOF particles and bare FTO squares. Scale bar is 500 μm; b) fluorescence microscopy image of the same patterned film upon excitation with a 405 nm laser irradiation, showing the blue color resulting from the emission of the pyrene ligands; c) an higher magnification SEM image of the patterned MOF film, scale bar is 100 μm; d) XRD of patterned NU-1000 covered with UiO-66 film (black), exhibiting diffraction peaks matching both simulated patterns of NU-1000 (red) and UiO-66 (blue); e) SEM image of UiO-66 deposited on top of the patterned NU-1000 thin film, creating a mix structure of NU-1000/UiO-66 film.

pattern not shown). Finally, EPD was tested and shown to be capable of producing more complex MOF film designs, as shown in the Table of Contents illustration.

The versatility of the EPD method was further demonstrated through the fabrication of a patterned thin film containing two types of MOF. Briefly, an EPD grid-patterned film of NU-1000 on conductive glass was immersed in a toluene suspension of UiO-66 and subjected to a DC potential as described above. The result was electrophoretic deposition of UiO-66 particles over both the exposed FTO areas and the pre-existing grid of NU-1000 particles; see Figures 4e and **S8**. The PXRD pattern of the mixed-MOF film, shown in Figure 4c, exhibits diffraction peaks for both NU-1000 (2θ = 2.4, 5.1) and UiO-66 (2θ = 7.3, 8.4).

In summary, we find that electrophoretic deposition is a simple and compelling method for assembling nanoparticulate thin-films of MOFs on conductive surfaces, including the assembly of films in micropatterned form. Successful deposition of four nominally neutral MOFs strongly suggests that EPD will prove applicable to a very broad range of MOF compositions. At high surface coverage, films of the redox-active MOF, NU-1000, proved to be fully electrochemically addressable—clearly an advantageous property for applications such as electrocatalysis for alternative fuel generation (water oxidation, hydrogen evolution reaction and CO_2 reduction) and chemical/electrochemical sensing. Going forward, we believe that EPD will open up a path for constructing more complex and multifunctional surface architectures comprising of multiple MOF materials. This multiplexing may prove useful in mechanistic investigation of important fundamental MOF properties such as charge transport and electrical conductivity.

Supporting Information

Supporting Information is available from the Wiley Online Library or from the author.

Acknowledgements

J.T.H. gratefully acknowledge support, respectively, from Northwestern University and the U.S. Dept. of Energy, Office of Science, Basic Energy Science program (grant no. DE-FG87ER13808). O.K.F gratefully acknowledges funding from the Army Research Office (project number W911NF-13-1-0229). I.H. thanks the U.S–Israel Fulbright program for a postdoctoral fellowship.

Received: April 30, 2014
Revised: June 15, 2014
Published online: July 28, 2014

[1] G. Ferey, *Chem. Soc. Rev.* **2008**, *37*, 191.
[2] H. Furukawa, K. E. Cordova, M. O'Keeffe, O. M. Yaghi, *Science* **2013**, *341*, 974.
[3] S. T. Meek, J. A. Greathouse, M. D. Allendorf, *Adv. Mater* **2011**, *23*, 249.
[4] C. E. Wilmer, M. Leaf, C. Y. Lee, O. K. Farha, B. G. Hauser, J. T. Hupp, R. Q. Snurr, *Nat. Chem.* **2012**, *4*, 83.
[5] O. K. Farha, A. O. Yazaydin, I. Eryazici, C. D. Malliakas, B. G. Hauser, M. G. Kanatzidis, S. T. Nguyen, R. Q. Snurr, J. T. Hupp, *Nat. Chem.* **2010**, *2*, 944.
[6] O. K. Farha, I. Eryazici, N. C. Jeong, B. G. Hauser, C. E. Wilmer, A. A. Sarjeant, R. Q. Snurr, S. T. Nguyen, A. O. Yazaydin, J. T. Hupp, *J. Am Chem. Soc.* **2012**, *134*, 15016.
[7] H. Furukawa, N. Ko, Y. B. Go, N. Aratani, S. B. Choi, E. Choi, A. O. Yazaydin, R. Q. Snurr, M. O'Keeffe, J. Kim, O. M. Yaghi, *Science* **2010**, *329*, 424.
[8] R. Grunker, V. Bon, P. Muller, U. Stoeck, S. Krause, U. Mueller, I. Senkovska, S. Kaskel, *Chem. Commun.* **2014**, *50*, 3450.
[9] J. R. Li, J. Sculley, H. C. Zhou, *Chem. Rev.* **2012**, *112*, 869.
[10] L. Q. Ma, C. Abney, W. B. Lin, *Chem. Soc. Rev.* **2009**, *38*, 1248.
[11] J. Lee, O. K. Farha, J. Roberts, K. A. Scheidt, S. T. Nguyen, J. T. Hupp, *Chem. Soc. Rev.* **2009**, *38*, 1450.
[12] C. Wang, Z. G. Xie, K. E. deKrafft, W. L. Lin, *J. Am Chem. Soc.* **2011**, *133*, 13445.
[13] L. E. Kreno, K. Leong, O. K. Farha, M. Allendorf, R. P. Van Duyne, J. T. Hupp, *Chem. Rev.* **2012**, *112*, 1105.
[14] G. Ferey, F. Millange, M. Morcrette, C. Serre, M. L. Doublet, J. M. Greneche, J. M. Tarascon, *Angew. Chem. Int. Ed.* **2007**, *46*, 3259.
[15] R. Diaz, M. G. Orcajo, J. A. Botas, G. Calleja, J. Palma, *Mater. Lett.* **2012**, *68*, 126.
[16] C. W. Kung, T. C. Wang, J. E. Mondloch, D. Fairen-Jimenez, D. M. Gardner, W. Bury, J. M. Klingsporn, J. C. Barnes, R. Van Duyne, J. F. Stoddart, M. R. Wasielewski, O. K. Farha, J. T. Hupp, *Chem. Mater.* **2013**, *25*, 5012.
[17] C. R. Wade, M. Y. Li, M. Dinca, *Angew. Chem. Int. Ed.* **2013**, *52*, 13377.
[18] A. Betard, R. A. Fischer, *Chem. Rev.* **2012**, *112*, 1055.
[19] S. Hermes, F. Schroder, R. Chelmowski, C. Woll, R. A. Fischer, *J. Am Chem. Soc.* **2005**, *127*, 13744.
[20] E. Biemmi, C. Scherb, T. Bein, *J. Am Chem. Soc.* **2007**, *129*, 8054.
[21] D. Van Gough, T. N. Lambert, D. R. Wheeler, M. A. Rodriguez, M. T. Brumbach, M. D. Allendorf, E. D. Spoerke, *ACS Appl. Mater. Interfaces* **2014**, *6*, 1509.
[22] M. C. So, S. Jin, H. J. Son, G. P. Wiederrecht, O. K. Farha, J. T. Hupp, *J. Am. Chem. Soc.* **2013**, *135*, 15698.
[23] O. Shekhah, *Materials* **2010**, *3*, 1302.
[24] O. Shekhah, H. Wang, M. Paradinas, C. Ocal, B. Schupbach, A. Terfort, D. Zacher, R. A. Fischer, C. Woll, *Nat. Mater* **2009**, *8*, 481.
[25] M. Y. Li, M. Dinca, *J. Am. Chem. Soc.* **2011**, *133*, 12926.
[26] M. Y. Li, M. Dinca, *Chem. Sci.* **2014**, *5*, 107.
[27] R. Ameloot, L. Stappers, J. Fransaer, L. Alaerts, B. F. Sels, D. E. De Vos, *Chem. Mater* **2009**, *21*, 2580.
[28] S. Yadnum, J. Roche, E. Lebraud, P. Négrier, P. Garrigue, D. Bradshaw, C. Warakulwit, J. Limtrakul, A. Kuhn, *Angew. Chem.* **2014**, *53*, 1.
[29] Y. Yoo, H. K. Jeong, *Chem. Commun.* **2008**, 2441.
[30] P. Horcajada, C. Serre, D. Grosso, C. Boissiere, S. Perruchas, C. Sanchez, G. Ferey, *Adv. Mater* **2009**, *21*, 1931.
[31] L. Grinis, S. Dor, A. Ofir, A. Zaban, *J. Photochem. Photobiol. A* **2008**, *198*, 52.
[32] A. Salant, M. Shalom, I. Hod, A. Faust, A. Zaban, U. Banin, *ACS Nano.* **2010**, *4*, 5962.
[33] E. M. Wong, P. C. Searson, *Appl. Phys. Lett.* **1999**, *74*, 2939.
[34] S. V. Mahajan, S. A. Hasan, J. Cho, M. S. P. Shaffer, A. R. Boccaccini, J. H. Dickerson, *Nanotechnology* **2008**, 19.
[35] S. V. Mahajan, J. Cho, M. S. P. Shaffer, A. R. Boccaccini, J. H. Dickerson, *J. Eur. Ceram. Soc.* **2010**, *30*, 1145.
[36] R. C. Bailey, K. J. Stevenson, J. T. Hupp, *Adv. Mater.* **2000**, *12*, 1930.
[37] M. Giersig, P. Mulvaney, *J. Phys. Chem.* **1993**, *97*, 6334.

[38] T. Teranishi, M. Hosoe, T. Tanaka, M. Miyake, *J. Phys. Chem. B.* **1999**, *103*, 3818.
[39] B. Ferrari, A. Bartret, C. Baudin, *J. Eur. Ceram. Soc.* **2009**, *29*, 1083.
[40] J. Cihlar, D. Drdlik, Z. Cihlarova, H. Hadraba, *J. Eur. Ceram. Soc.* **2013**, *33*, 1885.
[41] J. E. Mondloch, W. Bury, D. Fairen-Jimenez, S. Kwon, E. J. DeMarco, M. H. Weston, A. A. Sarjeant, S. T. Nguyen, P. C. Stair, R. Q. Snurr, O. K. Farha, J. T. Hupp, *J. Am. Chem. Soc.* **2013**, *135*, 10294.
[42] M. J. Katz, Z. J. Brown, Y. J. Colon, P. W. Siu, K. A. Scheidt, R. Q. Snurr, J. T. Hupp, O. K. Farha, *Chem. Commun.* **2013**, *49*, 9449.
[43] S. S. Y. Chui, S. M. F. Lo, J. P. H. Charmant, A. G. Orpen, I. D. Williams, *Science* **1999**, *283*, 1148.
[44] T. Loiseau, C. Serre, C. Huguenard, G. Fink, F. Taulelle, M. Henry, T. Bataille, G. Ferey, *Chem.-Eur. J.* **2004**, *10*, 1373.
[45] H. Wu, T. Yildirim, W. Zhou, *J. Phys. Chem. Lett.* **2013**, *4*, 925.
[46] J. H. Cavka, S. Jakobsen, U. Olsbye, N. Guillou, C. Lamberti, S. Bordiga, K. P. Lillerud, *J. Am. Chem. Soc.* **2008**, *130*, 13850.
[47] K. E. deKrafft, W. S. Boyle, L. M. Burk, O. Z. Zhou, W. B. Lin, *J. Mater. Chem.* **2012**, *22*, 18139.
[48] F. Vermoortele, R. Ameloot, A. Vimont, C. Serre, D. De Vos, *Chem. Commun.* **2011**, *47*, 1521.
[49] L. J. Shen, S. J. Liang, W. M. Wu, R. W. Liang, L. Wu, *J. Mater Chem. A* **2013**, *1*, 11473.
[50] M. J. Katz, J. E. Mondloch, R. K. Totten, J. K. Park, S. T. Nguyen, O. K. Farha, J. T. Hupp, *Angew. Chem. Int. Edit.* **2014**, *53*, 497.
[51] M. D. Allendorf, A. Schwartzberg, V. Stavila, A. A. Talin, *Chem.-Eur. J.* **2011**, *17*, 11372.
[52] A. A. Talin, A. Centrone, A. C. Ford, M. E. Foster, V. Stavila, P. Haney, R. A. Kinney, V. Szalai, F. El Gabaly, H. P. Yoon, F. Leonard, M. D. Allendorf, *Science* **2014**, *343*, 66.
[53] L. Sun, T. Miyakai, S. Seki, M. Dinca, *J. Am. Chem. Soc.* **2013**, *135*, 8185.